Structure and enhanced magnetization in Fe/Pt multilayers

A. Simopoulos, E. Devlin, and A. Kostikas
Institute of Materials Science, National Center for Scientific Research Demokritos, 15310 Ag. Paraskevi, Athens, Greece

Alan Jankowski
Lawrence Livermore National Laboratory, Livermore, California 94550

Mark Croft
Department of Physics, Rutgers University, Piscataway, New Jersey 08855-0909

Thomas Tsakalakos
Department of Ceramics, Rutgers University, Piscataway, New Jersey 08855-0909
and Institute of Materials Science, National Center for Scientific Research Demokritos, 15310 Aghia Paraskevi, Athens, Greece
(Received 26 February 1996; revised manuscript received 31 May 1996)

A series of Fe/Pt multilayers, prepared by magnetron sputtering, were characterized by structural [x-ray diffraction (XRD), x-ray-absorption spectroscopy, extended x-ray-absorption fine structure, TEM] and magnetization techniques and extensively investigated by Mössbauer spectroscopy. The Fe layer thickness varied from 3 to 60 Å and that of Pt from 5 to 39 Å. The 3 Å Fe/9 Å Pt sample displays magnetic hyperfine structure at room temperature (RT) while the 3 Fe/19 Pt sample is paramagnetic at RT, demonstrating the effect of the interlayer interaction. Both samples display out of plane magnetic anisotropy with a 39° angle with respect to the normal for the former and 20° for the latter. As the Fe layer thickness increases the magnetic vector turns to the plane. Systematic analysis of the Mössbauer spectra of samples with increasing Fe layer thickness allowed the determination of the magnetic hyperfine field for each Fe monolayer within the Fe layer slab. Hyperfine fields larger than the bulk Fe value appear in all samples with Fe layer thickness larger than 3 Å, and display an oscillatory dependence on the distance of the corresponding Fe monolayer from the interface. These hyperfine field values scale linearly with the average interplanar distance of the Fe layer derived from the refinement of the XRD data for each sample. Fe atomic magnetic moments determined from superconducting quantum interference device magnetometry and Rutherford backscattering spectroscopy measurements are also larger than the bulk Fe value, approaching it for large Fe layer thickness. The parameters determining the enhancement of magnetization in the Fe/Pt system are discussed. [S0163-1829(96)03538-2]

I. INTRODUCTION

Magnetic multilayers have been extensively studied during the past few years both for their potential in magnetic storage technologies and for their scientific interest as new artificial materials on the nanometer scale. Among the primary questions that have been addressed are the perpendicular magnetic anisotropy and its relation with interface phenomena, the modification of the atomic magnetic moment and the magnetic hyperfine field at the interface and neighboring atomic layers, and the intralayer and interlayer exchange interactions.

An interesting class of magnetic multilayers consists of successive identical bilayers with one magnetic and one nonmagnetic component. Such systems are the Fe/Au and Fe/Ag multilayers with nearly zero magnetization in the noble metal component, and multilayers of Fe with the ''nearly magnetic'' Pd or Pt metals. Strong polarization effects are expected close to the interface in the latter class of multilayers. Recently, by using the ''one monolayer probe'' Mössbauer technique, Kisters *et al.*[1] were able to determine the variation of the magnetic hyperfine field of the Fe monolayers below the interface in the Fe/Pd system. The hyperfine field follows a damped oscillation with a maximum at the first monolayer below the interface corresponding to a ~12% enhancement with respect to the bulk iron value. A similar enhancement has been predicted theoretically by Freeman and Fu[2] for a free standing nine layer iron slab. Recently, similar calculations have been performed for Fe/Pt multilayers with a combination of 5 Fe and 4 Pt monolayers.[3]

Extensive studies of the magnetic properties of Fe/Pt multilayers grown along the ⟨111⟩ direction[4] or the ⟨001⟩ direction[5,6] have been reported. These studies have concentrated on the investigation of perpendicular magnetic anisotropy and its relation with the local structure. Mössbauer studies have been also reported on two ultrathin Fe/Pt samples by Brand *et al.*[7]

We report in this paper detailed studies on structural and magnetic characterization on a set of ultrathin and thin Fe/Pt multilayers grown along the ⟨111⟩ direction with varying thicknesses of the Fe and Pt components. Magnetic circular dichroism studies have been reported for these samples,[8] as well as preliminary magnetization and Mössbauer studies.[9]

Among the principal aims of the present work is the determination of the atomic magnetic moment and the magnetic hyperfine field for each atomic monolayer of Fe in the Fe/Pt bilayer. The experimental technique of choice for this purpose is Mössbauer spectroscopy. It has been applied

TABLE I. Layer thicknesses t and interplanar spacings d of the Fe/Pt multilayers in Å. N: number of periods; μ: average atomic moments of Fe in Bohr magnetons; b: spin-wave stiffness constant.

Sample	N	t_{Fe}	t_{Pt}	$t^{XTC}_{Fe/Pt}$	$t^{XRD}_{Fe/Pt}$	d_{Fe}	d_{Pt}	$d^{XRD}_{\langle 111\rangle}$	μ	b 10^{-5} K$^{-3/2}$
Bulk Pt⟨111⟩								2.27		
3/39	44	3.1	38.8	41.9	42.4			2.27		
3/19	76	3.1	19.4	22.5	22.3			2.27		
3/9	135	3.0	9.7	12.7	12.8			2.26		
5/9	110	5.3	9.4	14.7	13.5			2.23	3.2	3.4
7/9	100	7.1	9.3	16.4	15.3	2.207±0.005	2.236±0.005	2.22	2.7	2.7
9/14	60	9.4	13.9	23.3	21.9	2.186	2.249	2.22	2.9	4.5
9/9	92	9.5	9.5	19.0	20.1	2.176	2.217	2.19	2.6	2.5
12/9	75	12.4	9.3	21.7	21.2	2.144	2.229	2.17	2.7	1.8
9/5	100	9.3	4.7	14.0	14.0	2.148	2.163	2.16	2.8	1.8
25/9	45	24.7	8.7	33.4	33.2	2.092	2.200	2.11	2.7	
38/9	33	38.4	9.4	47.8	46.9	2.062	2.226	2.09	2.5	
60/9	24	60.5	8.9	69.4	70.6	2.045	2.222	2.06	2.3	
Bulk Fe⟨110⟩								2.03	2.2	0.52

in the past by probing one or two individual monolayers with Fe^{57} enrichment in clean Fe film[10] and Fe/Pd bilayers.[1] Although this technique is efficient, it presents some drawbacks regarding the high cost of sample preparation and the interdiffusion between Fe^{56} and Fe^{57} isotopes. In the present work we studied a set of samples with constant Pt thickness and a stepwise increasing Fe thickness, allowing in this way the determination of the contribution of each additional Fe monolayer. These results are discussed in the framework of recent band structure calculations and semiempirical models.

We have also studied a set of samples with constant Fe and varying Pt thickness in order to determine the effect of interlayer exchange interactions between the magnetic Fe layers. We chose for this purpose samples with thin Fe layer thickness (1–2 monolayers) where the effect of perpendicular magnetic anisotropy is expected to be more pronounced.

Another aspect which is of considerable interest is the effect of the local structure on the magnetic properties of each individual monolayer. It has been suggested[11] and investigated experimentally[12,13] that under favorable conditions, an fcc phase forms in Fe thin films or multilayers with a ''high spin'' Fe moment. Such structural transformations from bcc to fcc Fe have been observed in Fe/Pt multilayers grown in the ⟨100⟩ direction.[5] In order to investigate the possibility of such a ''high spin'' phase in our systems we have performed extensive polarized x-ray-absorption spectroscopy (XAS) and extended x-ray-absorption fine-structure (EXAFS) measurements.

II. SAMPLE PREPARATION

The multilayer samples were prepared using magnetron sputter deposition. The deposition chamber was cryogenically pumped to a base pressure of 1.3×10^{-5} Pa. A circular array of magnetron sources was situated 20 cm beneath an oxygen-free copper platen. The magnetron sources are operated in the dc mode at a 330–390 V discharge. An argon working pressure of 0.40 Pa was used at a flow rate of 15.5 cm^3/min. The substrates were sequentially rotated over each source at 1.0 rev/min. The target materials were >0.9994 pure. The polished (Si and mica) substrates were cleaned with a procedure consisting of detergent wash, deionized water rinse, alcohol rinse and a $N2$ gas drying prior to deposition. The substrates remained at a temperature between 293 and 306 K during the deposition. The sputter deposition rates, between 0.2 and 5 Å per sec, were monitored using calibrated quartz crystals (XTC's). The quartz crystals provide the component layer thickness for iron (t_{Fe}) and platinum (t_{Pt}) as well as the layer pair thickness ($t_{Fe/Pt}-$XTC). The multilayer films were grown to a 2000 Å total thickness consisting of N layer pairs. Table I gives a list of the samples with the individual component thicknesses (t_{Fe},t_{Pt}), the layer pair thicknesses ($t_{Fe/Pt}$, derived from XTC and XRD, respectively) and the interplanar spacings, derived from the x-ray diffraction peaks ($d_{\langle 111\rangle}-$XRD) and their respective analysis (d_{Fe},d_{Pt}; see next section). Each sample is designated in this table and in the text by two numbers which are the Fe and Pt layer thicknesses to the nearest Å.

III. STRUCTURAL CHARACTERIZATION

X-ray diffraction (XRD), transmission electron microscopy (TEM), XAS, EXAFS, and Rutherford backscattering (RBS) have been employed for the structural characterization of the multilayer samples. Some results of the first two techniques have been published recently[8] and are presented here as summary results for the sake of completeness.

X-ray diffraction. Both in-house and synchrotron based x-ray diffraction facilities were utilized to determine the structure and structural parameters of the multilayers. A powder diffractometer equipped with a graphite monochromator was used in the $\theta-2\theta$ mode at both low and high angles using Cu Ka radiation. The x-ray diffraction measurements show fcc-Pt-[111] structure with sharp low and high angle superlattice satellites. The lattice spacings are computed from the reflected peak positions via Bragg's law (Table I). The grazing incidence scans of the multilayer films (Fig. 1) reveal satellite reflections above (000) attributable to the composition modulation in the multilayer growth direction.

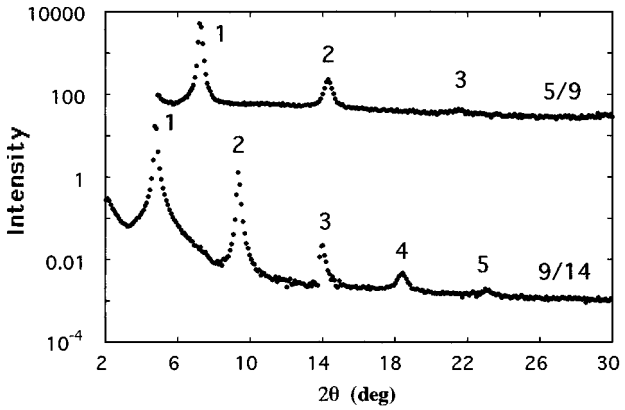

FIG. 1. X-ray diffraction in the low angle region for the 5/9 and 9/14 samples.

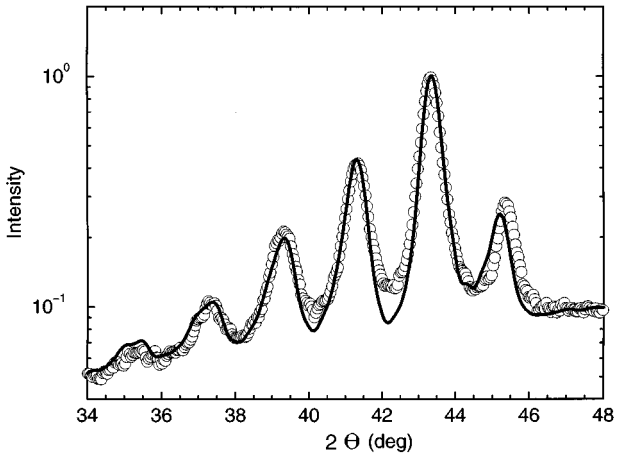

FIG. 2. X-ray diffraction in the high angle region for the 38/9 sample fitted with the structural refinement procedure (bold line).

In the low angle region the analysis is made by an optical formalism which takes into account the interface roughness, the critical angle, and the wave vector of the reflectivity. Figure 1 shows representative low-angle diffraction spectra in which satellite intensities up to fifth order are observed, indicative of the high quality of the multilayers. From the intensity ratios of different orders of satellites the roughness was estimated to be 2–5 Å, which corresponds to a value of one to two monolayers.

In the high-angle x-ray-diffraction spectra a complete quantitative characterization of the Fe-Pt superlattices was performed by multidimensional optimization of a stochastic model, where the structural parameters of the superlattice were refined. The detailed structural information determined by this model fitting includes the following: grain size and grain size distributions; the thickness of the individual layers and thickness fluctuations; roughness, interdiffusion, and lattice strains; and finally the average d spacings of the individual Fe and Pt layers. Details of the analysis and the theoretical foundation of the structural refinement procedure are given in Ref. 14. Examples of the experimental and refined-model high-angle x-ray spectra for the 38/9 Fe/Pt multilayer are shown in Fig. 2. As can be seen, the Bragg peak of the average lattice is flanked by four low-angle satellites and only one high-angle satellite, all of which are fitted very satisfactorily by the structural refinement model. The refined parameters for this sample are in excellent agreement with nominal processing parameters. Table I contains the average d spacings d_{Fe} and d_{Pt}, derived from the structural refinement procedure. We notice an increase of d_{Fe} as the Fe layer thickness decreases. The refinement data show also that the interdiffusion is limited to the first two monolayers from the interface.

Transmission electron microscopy. TEM and high resolution imaging reveal the Fe/Pt multilayer film morphology and lattice structure. The plan-view electron diffraction patterns [Fig. 3(a)] demonstrate the polycrystalline in-plane nature of the film with a 5–8° mosaic of the lattice planes perpendicular to the textured {111} growth direction. The ring pattern for the sample 9/9, shown in Fig. 3(b), yields a mean in-plane lattice parameter of 3.84 Å. Selected area diffraction of individual grains, viewed in cross section have been published elsewhere[8] and clearly showed the {111} growth direction of the multilayer. The film growth structure imaged in cross section is found to be typified by densely packed columns with an average in-plane grain size of 270–300 Å. High resolution lattice image of a single columnar grain, recorded at the Scherzer defocus condition using a 400 keV electron beam, is shown in Fig. 4.

X-ray-absorption spectroscopy. Fe-K-edge XAS measurements were carried out on beamline X-19A at the Brookhaven National Light Source. The beamline optics consists of a double crystal (Si-111 and Si-220) monochromator along with vertical-parallelization and horizontal-focusing parabolic Rh mirrors. The data were collected in the fluorescence mode using a Canberra Si-PIPS detector. Al-

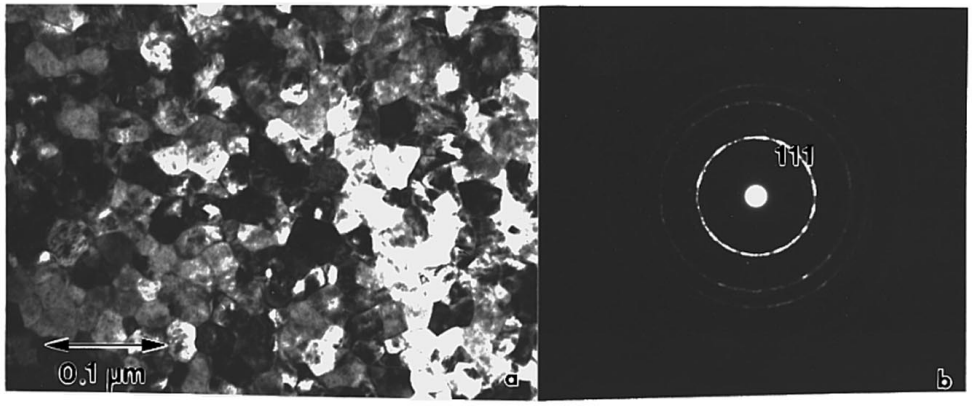

FIG. 3. Conventional transmission electron microscopy of sample 9/9, as imaged in plan view, reveals (a) the fine grain size in the bright field image and (b) the preferred {111} texture in the electron diffraction pattern of the film.

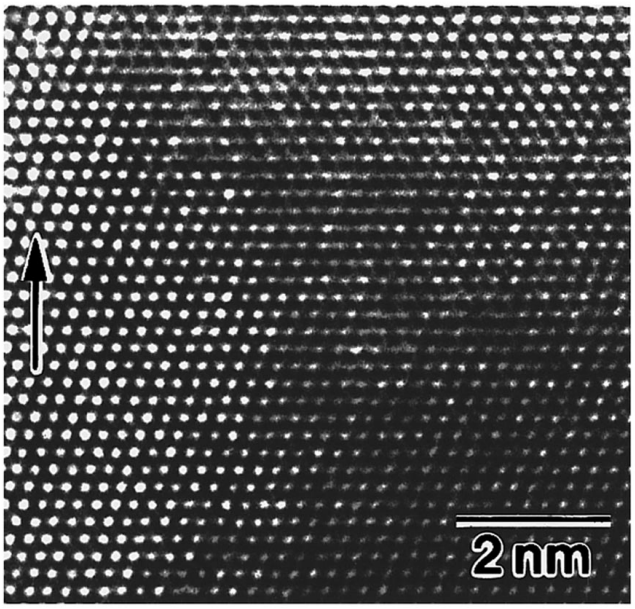

FIG. 4. High resolution electron micrograph of the sample 9/9, as imaged in cross section. The growth direction is indicated by an arrow.

though XAS results were obtained for beam polarizations oriented both in- and perpendicular-to-the multilayer slabs, only the in-plane results are reported here.

Selected results are presented here [see Figs. 5(a) and 5(b)] for the near edge XAS spectra and for the pseudoradial distribution function (PRDF). The PRDF reflects the backscattering from the various neighboring atomic shells and is the Fourier transform of the oscillatory component of the absorption coefficient above the edge. Details of the XAS analysis, modeling, and the Fe layer fcc to bcc crossover will be presented elsewhere.[15]

The XAS measurements revealed a systematic crossover in the Fe-layer structure from fcc, in the thin Fe-layer thickness limit, to bcc in the thick Fe-layer limit. A number of studies of Fe materials have shown that a bimodal first near edge peak [e.g., see the two arrows under the 7/9 spectrum in Fig. 5(a)] is an indicator of fcc structure and that a single first peak [e.g., see single arrow under the 38/9 spectrum in Fig. 5(a)] is an indicator of the bcc structure. The spectrum of the 9/14 sample on the other hand appears to be on the border line of the fcc to bcc crossover. The fcc to bcc structure change is also reflected by the qualitative changes in the absorption coefficient oscillations over the 130 eV above the edge [Fig. 5(a)]. It is worth noting that the presumed stacking in the Fe layers is ⟨110⟩.

The PRDF address these fine structure oscillations changes over a wider range and in a way related more directly to the atomic shell structure. The PRDF results reflect the fcc to bcc change by the first-shell-peak-shift $s1$ [Fig. 5(b)] and by the change in the most prominent higher shell feature from the fcc-third-shell $s3$ (opposite face center atoms) to the bcc-fourth-shell $s4$ (adjacent cell body center atoms). Thus the PRDF of the thick-Fe 38/9 sample is basically the same with that of bcc-Fe with the strong 24-coordinate fourth atomic shell [labeled $s4$ in Fig. 5(b)]. The 9/5 sample shows also the strong $s4$-bcc feature indicating a

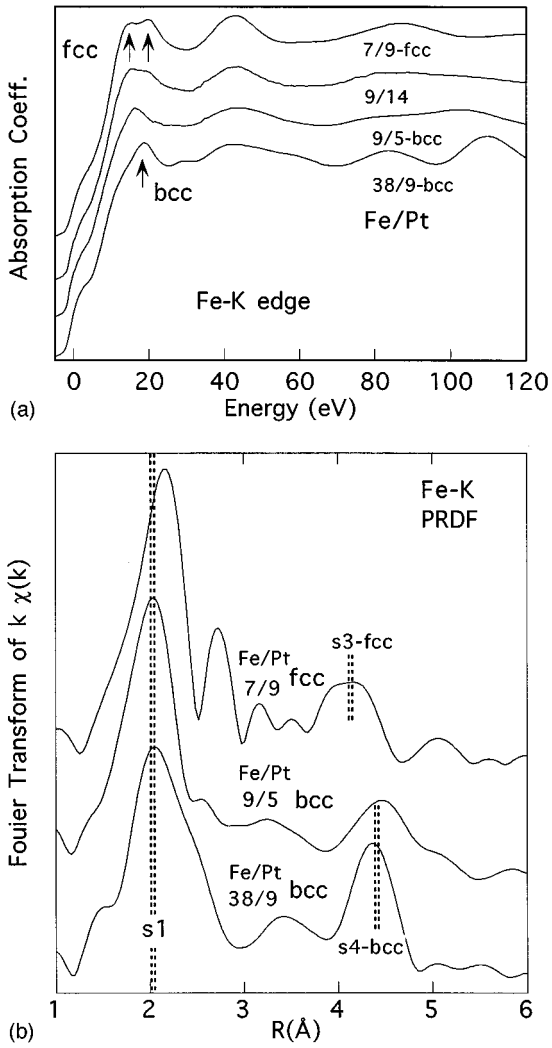

FIG. 5. (a) The Fe-K spectra of 7/9, 9/14, 9/5, and 38/9 Fe/Pt samples. (b) The Fe-K pseudoradial-distribution-function (PRDF) results for 7/9, 9/5, and 38/9 Fe/Pt samples.

bcc structure. Moreover, the first atomic shell ($s1$) PRDF of this sample occurs at the same position as the 38.9 feature supporting the bcc assignment. The PRDF curve for the 7/9 sample on the other hand evidences the crossover to fcc-Fe-layer structure: a first shell peak shifted to higher distance and a higher shell peak typical of the 24 coordinate third shell in the fcc structure ($s3$-fcc).

Rutherford backscattering. RBS measurements were performed in order to determine the atomic area densities for the Fe and Pt components. These densities combined with the saturation magnetization data of the corresponding samples allowed us to determine the magnetic moment per Fe atom for the Fe/Pt samples as will be discussed in the next section.

IV. MAGNETIC CHARACTERIZATION

A. Magnetic measurements

Magnetization data were taken with a superconducting quantum interference device (SQUID) magnetometer at temperatures between 4.2 and 300 K. Figure 6 displays magnetization graphs for the samples with ~1.5 Fe monolayer (ML) thickness (~3 Å) in film directions parallel and per-

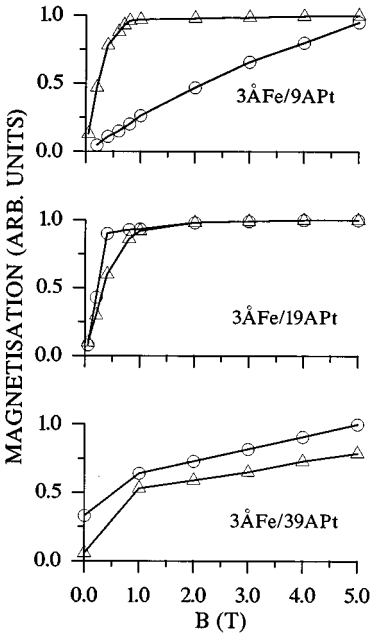

FIG. 6. Magnetization curves at 10 K in directions parallel (triangles) and perpendicular (circles) to the film plane for the 3/9, 3/19, and 3/39 samples.

pendicular to the magnetizing field. A change of the anisotropy out of the plane is shown for the samples with larger Pt layer thickness (3/19 and 3/39 samples) while the 3/9 sample displays an easy axis of magnetization parallel to the plane of the film. The same orientation of the magnetic moment is displayed for the samples with larger Fe thickness layers. An apparent lack of saturation even in a field of 5 T is shown in the data of the 3/39 sample. This may be attributed to more pronounced two-dimensional character for this sample, due to the large separation of the Fe layers, and thus more pronounced anisotropy, although the poor signal to noise ratio for this sample due to the small quantity of Fe does not allow a final conclusion.

The temperature variation of the saturation magnetization is displayed in Fig. 7. This variation is faster than that displayed in bulk iron with a slope increasing as the Fe thickness decreases and the Pt thickness increases. From the temperature variation of the magnetization we determined the spin-wave stiffness constant b from the Bloch equation:

$$M_s(T) = M_0(1 - bT^{3/2}).$$

It should be noted that the magnetization data of sample 3/9 follow closely the $T^{3/2}$ dependence while the data of the samples 3/19 and 3/39 are well fitted with a linear temperature expression. The variation of the spin-wave stiffness constant b with the thickness of the Fe(Pt) component for the thin Fe/Pt samples is listed in Table I. The values of the ultrathin samples are not included in this table since they follow a different temperature variation and therefore cannot be directly compared with the corresponding parameter values of the rest of the samples. The b parameter values are considerably larger than those of α-Fe for small Fe layer thicknesses, approaching the bulk Fe value as the Fe thickness increases. The opposite effect is observed when the Pt thickness increases with constant Fe thickness.

We have also listed in Table I the magnetic moment per Fe atom for the various samples. These values were calculated as the ratio of the saturation magnetization measured at 4.2 K to the areal density of the Fe atoms (number of Fe atoms/cm^2), the latter being determined by the RBS data. These atomic magnetic moment values have been corrected by $0.3\mu_B$ which has been calculated[3] as the induced magnetic moment on the Pt atoms at the interface. It is obvious from this table that the Fe atomic magnetic moments in the multilayers are considerably larger than the bulk Fe value and decrease as the Fe layer thickness increases.

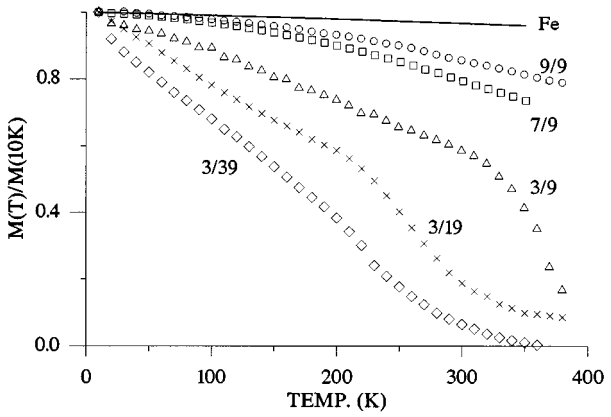

FIG. 7. Temperature dependence of the saturation magnetization of the Fe/Pt multilayers. The corresponding curve for bulk α-Fe is included for comparison.

B. Mössbauer measurements

Conversion electron Mössbauer spectra (CEMS) were taken at room temperature. Spectra taken in samples with the

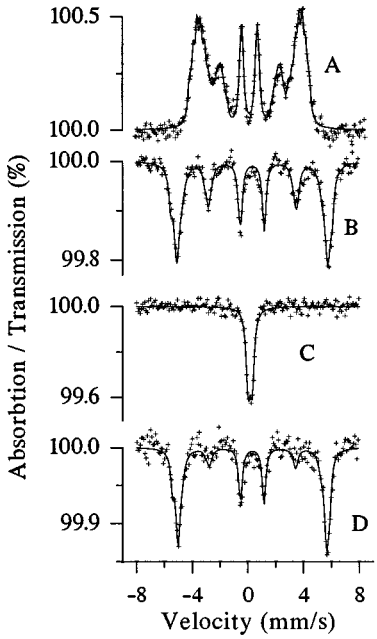

FIG. 8. Mössbauer spectra of the ultrathin Fe/Pt samples. (a) CEMS of the 3/9 sample at RT. (b) Transmission spectrum of the 3/9 sample at LHe temperature. (c) RT spectrum of the 3/19 sample. (d) LHe spectrum of the 3/19 sample. Solid lines represent least square fits.

TABLE II. Hyperfine parameters [i.s.: isomer shift with respect to Fe (mm/s); H: magnetic hyperfine field (kOe)] of the 3/9 and 3/19 Fe/Pt samples. Θ is the angle between the hyperfine field H and the normal to the film and A is the relative absorption of each component.

		Component I				Component II				Component III				
Sample	T (K)	i.s.	H	ΔH	A	i.s.	H	ΔH	A	i.s.	H	ΔH	A	Θ
3/9	300	0.25	250	13.5	23.3	0.28	227	13	51.0	0.28	199	13	25.7	39°±3°
	4.2	0.39	362	0.0	13.3	0.45	339	7	72.9	0.45	314	7	13.9	39°±3°
3/19	300	Linewidth $\Gamma=0.34$ mm/s, i.s.$=0.29$ mm/s, quadrupole splitting $e^2qQ/2=0.28$ mm/s												
	80	0.43	327	0.0	24.8	0.44	307	4	51.6	0.30	271	4	23.6	20°±5°
	4.2	0.36	352	0.0	18.0	0.45	333	4	70.8	0.40	310	4	11.2	20°±5°

same Fe/Pt combination but grown on mica or Si substrates were identical. For measurements at lower temperatures, transmission Mössbauer measurements were taken on the samples grown on mica after removing the mica substrate. (Mica has Fe impurities several times the Fe content of the multilayers.) In order to increase the signal to noise ratio, the films were cut in 1×1 cm squares which then were stacked together. Samples with 10–12 squares were used for these measurements. Transmission spectra of such samples taken at RT were identical to the corresponding CEMS spectra (i.e., fitted with the same model gave identical parameters) indicating that the removal of the mica substrate did not introduce any strain in the sample or affect the Fe hyperfine parameters in any way. The measurements were made in conventional constant acceleration Mössbauer spectrometers using a 60 mCi Co^{57}(Rh) source. Calibration of the spectrometers was done with a thin Fe film. We will present the data for three classes of Fe/Pt multilayers according to the thickness of the Fe component.

3 Å Fe/X Å Pt multilayers. These samples consist of 1–2 Fe monolayers and N Pt monolayers, N varying between 5 and 19. Figure 8 shows Mössbauer spectra for the 3/9 and 3/19 samples. Spectra for the 3/39 sample were not possible to take since the signal to noise ratio is too small for this sample. We notice first that the 3/9 sample displays magnetic hyperfine spectra already at RT while the 3/19 sample is paramagnetic at this temperature displaying magnetic hyperfine structure below 240 K. This difference indicates the reduction of the interlayer exchange interaction due to the greater nonmagnetic Pt thickness. The magnetization of both samples is out of the plane as witnessed by the reduced intensity of the $\Delta m=0$ lines. The angle between the direction of the hyperfine field $H_{\rm hf}$ and the normal to the plane, as determined by the ratio $\Delta m_{\mp 1}/\Delta m_0$, is 39° for the 3/9 sample and 20° for the 3/19 sample. The latter result is consistent with the linear temperature variation of the magnetization of the 3/19 sample indicating a two-dimensional behavior for this sample. Table II shows the results of the analysis of these spectra. The magnetically split spectra were analyzed with three components allowing for a small distribution of the hyperfine fields ΔH. Values larger than the corresponding value of bulk Fe (340 kOe) appear at LHe for both samples, while the hyperfine field distribution ΔH decreases at this temperature.

The analysis of the magnetically split spectra requires some further discussion. These two 1–2 Fe monolayer

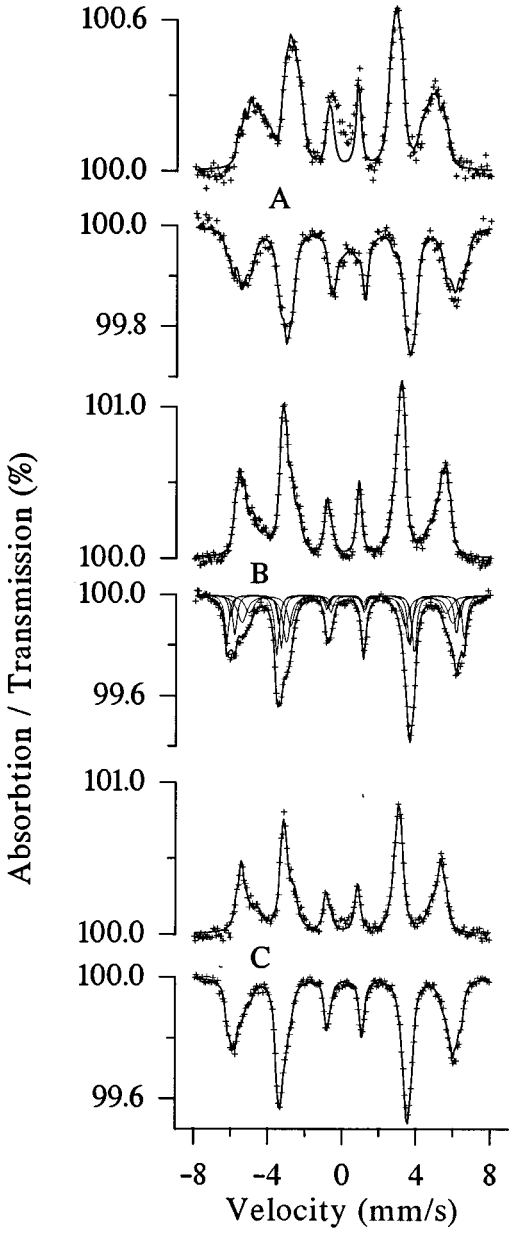

FIG. 9. Mössbauer spectra of the (a) 7/9, (b) 9/9, and (c) 12/9 samples. CEMS spectra (top) were recorded at RT and transmission spectra (bottom) at LHe. The misfit at the center of the CEMS 7/9 spectrum is due to contribution from Fe in mica. Spectral components are shown for the LHe spectrum of the 9/9 sample.

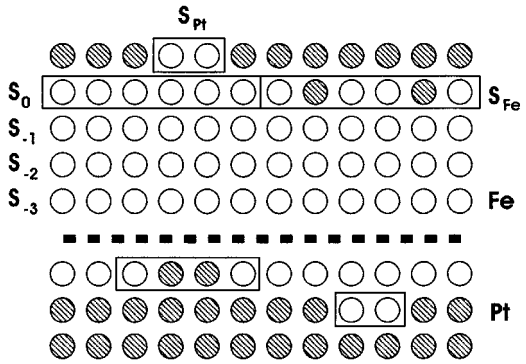

FIG. 10. Assumed structural model of the Fe/Pt structure used in the analysis of Mössbauer spectra. Open circles denote Fe atoms and shaded circles Pt atoms.

samples have a special morphology as compared to the thicker Fe samples to be described later. In the present case each Fe monolayer faces, at least from one side, a Pt layer. Furthermore, some interdiffusion is expected giving rise to a distribution of the hyperfine fields. The magnetically split spectra could also be fitted with a model similar to that applied for Fe alloys which was first introduced by Stearns.[16] In this model the hyperfine field and the isomer shift change linearly with the number of the nonmagnetic neighbors. Although good fits were achieved with this model we chose the three component fit for reasons of consistency with the model employed to fit the spectra of the thicker Fe samples which will be described next. It is worth noting however that the hyperfine fields and the isomer shift values listed in Table II are within the range of the values observed for bulk FePt disordered alloys[17,18] and they agree with the values determined by Brand *et al.*[8] for a 2 Fe/20 Pt multilayer.

X Fe/Y Pt (X: 5–12.5 Å;Y: 5–14 Å) multilayers. Taking that the interlayer distance is 2.2 Å for Fe and 2.3 Å for Pt, then these samples contain 2–6 Fe monolayers and ~2–6 Pt monolayers, respectively. Figure 9 shows Mössbauer spectra taken at RT and LHe with these samples in order of increasing Fe thickness. We notice first that they all display six-line patterns with inhomogeneous broadening which is reduced as the Fe thickness increases. The Δm_0 lines are larger than the outer $\Delta m_{\pm 1}$ lines indicating that the magnetic moments in these samples are in or near the film plane. After several attempts to fit these spectra in a consistent way, we settled with a fitting model employing up to five components, three of which were assigned to the interface (like in the case of the 1–2 Fe monolayer samples) and the remaining two to the Fe monolayers between the interfaces. This fitting model is based on the assumption that each Fe monolayer displays distinct hyperfine interactions depending on its distance from the interface. Assuming that each pair of the Fe monolayers which are at the same distance from the two respective interfaces are identical then, for this group of samples, we end up with two components, one corresponding to the monolayer underneath the interface (component S_{-1}) and one corresponding to the next Fe monolayer (component S_{-2}) as shown in Fig. 10. The expected contribution for each of these components in each spectrum is shown in the following table:

	Interface components	S_{-1}	S_{-2}
Sample 5/9	80%	20%	
Sample 7/9	57%	43%	
Sample 9/9	40%	40%	20%
Sample 12/9	33%	33%	33%

These values are correct under the assumption that there are no significant deviations in the films such as steps and/or diffusion beyond the interface.

Following the above description, the spectra were analyzed with four components for the 5/9 and 7/9 samples and with five components for the 9/*X* and 12/9 samples as shown in Table III. The fits were constrained to the instrumental linewidth (0.28 mm/s) for all the components. The relative intensity of each component was constrained to be the same for the spectra taken at RT and LHe with the exception of sample 9/14 for which satisfactory fits could not be achieved with this constraint. A distribution of hyperfine fields ΔH was allowed for the two of the three components (compo-

TABLE III. Hyperfine parameters of the *x* Fe/*y* Pt samples (*x*: 5–12 Å; *y*: 5–14 Å). Parameter symbols are the same as in Table II. Component symbols are described in the text.

		S_{-1}			S_{-2}			S_0			S_{Fe}			S_{Pt}		
Sample	T (K)	i.s.	H	A	i.s.	H	A	i.s.	H	A	i.s.	H	A	i.s.	H	A
5/9	300	0.09	351	8.7				0.08	321	13.8	0.10	291	46.1	0.14	254	31.4
	80	0.38	387	6.1				0.39	369	9.9	0.39	348	34.8	0.41	325	49.3
7/9	300	0.08	350	9.1				0.09	332	16.0	0.14	305	47.5	0.22	269	31.0
	4.2	0.30	408	7.3				0.33	388	13.8	0.38	360	40.1	0.40	330	26.5
9/9	300	0.12	359	22.0	0.10	346	11.0	0.13	334	19.4	0.19	310	27.9	0.31	280	19.7
	4.2	0.25	400.5	22.1	0.23	387	11.1	0.26	374	19.5	0.36	355	28.7	0.38	332	18.7
12/9	300	0.02	352	18.0	0.02	339	18.0	0.01	330	22.0	0.11	306	29.9	0.24	274	12.0
	4.2	0.25	394	18.0	0.23	380	18.0	0.23	367	21.9	0.29	350	30.2	0.36	326	11.9
9/5	300	0.04	362	18.6	0.06	345	9.3	0.04	341	20.6	0.08	330	30.4	0.23	301	21.1
	4.2	0.27	396	18.6	0.24	384	9.3	0.24	375	20.3	0.27	359	34.6	0.36	333	17.2
9/14	300	0.15	357	18.3	0.13	337	21.7	0.20	313	18.3	0.25	280	25.5	0.30	236	16.2
	4.2	0.26	395	14.8	0.28	383	7.4	0.25	369	14.8	0.38	348	39.3	0.39	318	23.6

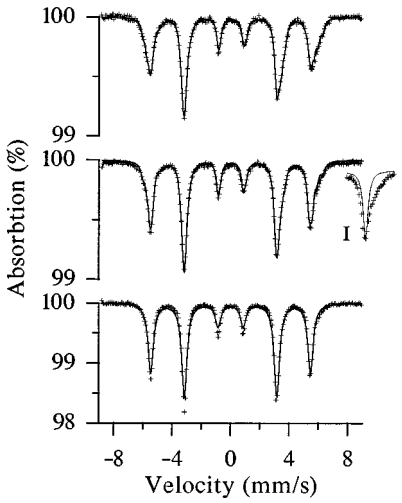

FIG. 11. Mössbauer spectra of the 25/9 (top), 38/9 (middle), and 60/9 (bottom) samples recorded at LHe. The insert **I** next to middle spectrum shows the absorption peak at ~5.5 mm/sec fitted with the corresponding bulk Fe line.

nents S_{Fe} and S_{Pt}) assigned to the interface in order to simulate the interdiffusion in the Fe and Pt monolayers. This distribution was ~10 kOe. The third component S_0 was assigned to parts of the interface Fe monolayer without Pt impurities (Fig. 10).

The results of the above analysis are shown in Table III. We notice first that the $S-1$ component appears with a hyperfine field larger than the bulk Fe value by 8% at RT and by 17% at LHe. This component appears already in the 5/9 sample where only a small fraction is expected for this monolayer. For this sample the intensity ratio of the $\Delta m_{\pm 1}$ and Δm_0 lines yields an angle of 68° for the direction of the magnetic moment relative to the vertical to the plane. This intensity ratio for the remaining samples is 3:4 in agreement with a planar direction of the magnetic moments for Fe layer thickness above 7 Å. Katayama *et al.*[4] arrived at a similar conclusion from magnetization measurements in Fe/Pt multilayers. The $S-2$ monolayer also displays hyperfine fields larger than bulk iron with an average value of 384 kOe at LHe and 342 kOe at RT. Similar enhancement of the hyperfine field is observed for the S_0 component, while the S_{Fe} and S_{Pt} components display smaller hyperfine field values due to the Pt impurities. Turning now to the isomer shift values we notice that they are all larger than the corresponding bulk iron values, both at RT and LHe, with a tendency to decrease as we move from the interface to the inner monolayer components. It is interesting to note that none of the components of this analysis displays hyperfine interaction parameters similar to the bulk iron values. We must also note that analysis of the Mössbauer spectra of the Fe/Pd system by Kisters *et al.*[1] gave similar results.

X Fe/9 Pt (X: 25, 38, and 60 Å) multilayers. These three ''thick'' Fe layer samples were examined in order to investigate further the variation of the hyperfine parameters as we move to deeper monolayers in the Fe layer. Figure 11 displays Mössbauer spectra of these samples at LHe. At first sight these spectra look like normal Fe calibration spectra with the magnetic moment in the plane (as witnessed by the 3:4:1 peak ratio), but a careful inspection shows some extra broadening in the wings. This is seen easier by fitting these spectra with one ''bulk iron'' component constrained to the instrumental linewidth (see inset of Fig. 11).

The sample with the thinnest Fe layer (sample 25/9) has six pairs of Fe monolayers corresponding to the interface pair and five symmetric pairs of monolayers between the interfaces. The Mössbauer spectra of this sample were fitted with the same model as the ''thin'' samples, extending the number of components up to the monolayer S_{-5}. The interface was approximated with two components, the S_0 and the $S_{Fe/Pt}$. The linewidths were constrained to the instrumental value and the intensities of the components beyond the S_{-1} were constrained to the relative abundances of the corresponding monolayer. The intensities of the interface and the S_{-1} components were left free to account for Pt diffusion. The results of this heavily constrained fit were rather satisfactory. As can be seen from Table IV the hyperfine parameters vary as we move from the interface to the center of the Fe layer approaching the bulk Fe values at the S_{-5} monolayer.

Following the same model and constraints we fitted the 38/9 and 60/9 samples incorporating the components corresponding to the extra monolayers (three and eight pairs, respectively) to the component S_{-5} which has reached the bulk hyperfine parameters. The results in Table IV show that there is a consistency of the hyperfine parameters displayed by the ''thick'' samples as compared with the parameters of the ''thin'' samples displayed in Table III. We notice again an enhancement of the magnetic hyperfine field for the S_{-1} and S_{-2} components, albeit smaller this time, and a decrease of the isomer shift as we move away from the interface, reaching the bulk iron value at the S_{-5} monolayer. We notice in particular an oscillation of the magnetic hyperfine field as we

TABLE IV. Hyperfine parameters of the *x* Fe/9 Pt samples (*x*: 24.7, 38.4, and 60.5 Å). Parameters symbols are the same as in Table II. Component symbols are described in the text.

Sample		S_{-1}			S_{-2}			S_{-3}			S_{-4}			S_{-5}			S_0			$S_{Fe/Pt}$		
	T (K)	i.s.	H	A	i.s.	H	A	i.s.	H	A	i.s.	H	A	i.s.	H	A	i.s.	H	A	i.s.	H	A
25/9	300	0.11	356	11	0.07	343	18	0.07	332	18	0.0	326	18	0.0	333	18	0.13	314	18	0.21	285	9
	4.2	0.27	383	11	0.23	365	18	0.19	352	18	0.12	335	18	0.13	343	18	0.24	337	18	0.25	315	9
38/9	300	0.11	351	9.6	0.10	335	11.5	0.00	328	26	0.00	333	26	0.0	331	26	0.04	322	26	0.20	289	6
	4.2	0.27	385	9	0.25	363	12	0.26	345	25	0.10	337	25	0.09	345	25	0.20	338	25	0.32	310	9
60/9	300	0.17	344	6	0.03	336	7	0.03	328.5	37	0.0	330	37	0.0	330	37	0.07	313	37	0.22	283	3
	4.2	0.27	377	6	0.25	358	7	0.27	343	36	0.11	341	36	0.11	340	36	0.17	332	36	0.32	305	3

move across the Fe layer in a similar fashion observed in the Fe/Pd case.[1] We will discuss the implications of these oscillations in the next section.

V. DISCUSSION

As we have described in the previous sections, the structure of the Fe/Pt films has been characterized by XRD and TEM and both these techniques point to good quality multilayers regarding growth in each grain along the ⟨111⟩ direction. The analysis of the XRD data indicates that deviations related to steps and roughness in each grain do not exceed one to two monolayers. The same holds for the interdiffusion between Fe and Pt at the interface.

Both the SQUID magnetometry and Mössbauer measurements show a dependence of the magnetic properties on the individual thickness of the Fe and Pt layer for each sample. In other words, the magnetic behavior of each sample seems to be determined by the number of Fe and Pt monolayers. Thus, in the case of ultrathin samples with one to two Fe monolayers, magnetic hyperfine interaction appears at RT for the 3/9 sample, while the magnetic transition temperature for the 3/19 sample is at ~240 K, manifesting the effect of the interlayer exchange interaction. A linear temperature variation of the magnetization is observed for the latter sample indicating a two-dimensional (2D) magnetic behavior due to the weak interlayer exchange interaction and a consequent loss of spin excitations across the film. The weak interlayer exchange also drives the magnetic vector to the normal to the film plane in this sample ($\Theta = 20° \pm 5°$) while as the number of Pt monolayers decreases or the number of Fe monolayers increases the magnetic vector turns to the plane ($\Theta = 39°$ for the 3/9 sample, 68° for the 5/9 sample, and 90° for all thicker Fe layer samples). Katayama *et al.*[4] and Brand *et al.*[7] arrived at similar conclusions regarding the perpendicular magnetic anisotropy.

We turn now to a discussion of the hyperfine parameters derived from the analysis of the Mössbauer spectra. Perhaps the most striking result is the appearance in these spectra of magnetic components with hyperfine fields with values of ~400 kOe at 4.2 K (Table IV). It is critical for the rest of the discussion to compare these large values with corresponding values observed in disordered FePt Invar alloys (Pt concentration: 25–35 %). Hesse *et al.*[17] have reported values ranging from 350–370 kOe with isomer shift values from 0.30–0.36 mm/sec, respectively. Similarly, Sumiyama *et al.*[18] observed hyperfine fields at 4.2 K ranging from 357–364 kOe in the same concentration range. These hyperfine field values, although large, are considerably smaller than the maximum values observed in the present study. Furthermore, the magnetic moments observed for the Invar alloys[18] are much smaller than the values of the Fe/Pt multilayers (Table I) and smaller than the bulk Fe values. Components with hyperfine parameters similar to the ones observed for the Invar alloys are observed in the spectra of the 3/9 and 3/19 samples (Table II), where the Fe-Pt interdiffusion could produce an environment similar to the Invar alloys. The same holds for the S_{Fe}, S_{Pt} components in the thicker Fe layer samples. These observations, together with the fact that the components $S0$, $S-1$, and $S-2$ have been constrained in the analysis to the instrumental linewidth without any distribution ΔH of hyperfine fields, indicate that the Fe-Pt interdiffusion is mostly at the first monolayer and the large hyperfine fields observed for the $S-1$, $S-2$ components is an inherent property of the Fe/Pt multilayers whose origin we will discuss next.

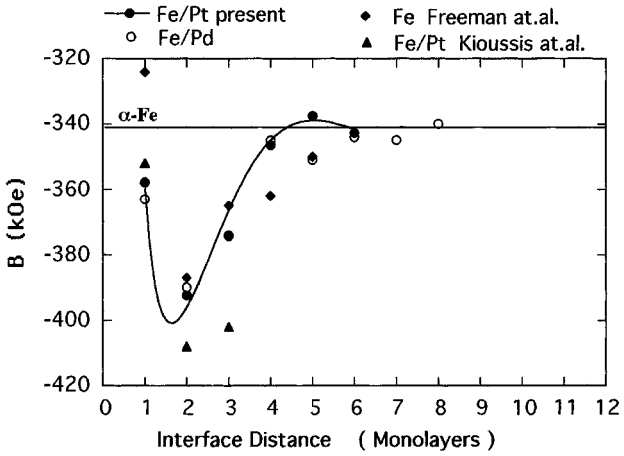

FIG. 12. Variation of the hyperfine field B assigned to each Fe monolayer with the distance from the interface. Experimental data are for Fe/Pt of the present study (full circles) and for Fe/Pd taken from Ref. 19. The solid line represents least square fit to the Fe/Pt data. Diamond and triangle symbols represent theoretical calculations.

As was mentioned already, Kisters *et al.*[1] have also observed large hyperfine fields in the Fe/Pd system by using the ''one monolayer probe'' Mössbauer technique. The hyperfine field values follow a damped oscillation as a function of the distance of the corresponding monolayer from the interface. They simulated their RT data with a semiempirical model employing a superposition of a short-range exponential distance dependence and a damped Ruderman-Kittel-Kasuya-Yosida (RKKY) like oscillating term. The important parameters in this fit are the range parameter δ which expresses the range of hybridization of the Fe-3d and the Pd-4d electron wave functions and the wavelength Λ of the RKKY term. These parameters were found equal to 1.65 and 4.43 ML's, respectively. We have plotted in Fig. 12 the hyperfine fields assigned to each Fe monolayer averaged over all the Fe/Pt samples we measured at LHe (Tables III and IV) together with the corresponding values of the Fe/Pd (Ref. 19) system. There is a striking similarity between these two sets of data as should be expected since both the Pd and the Pt counterparts of the Fe multilayers are both ''nearly magnetic'' metals. A fitting of the Fe/Pt data to the same semiempirical equation gives a hybridization range parameter $\delta = 1.50$ and the wavelength of the RKKY term $\Lambda = 4.95$ ML's.

We have also plotted in Fig. 12 calculated values by Freeman and Fu[2] for a free standing nine monolayer Fe slab. In this calculation they have employed the full-potential linearized augmented plane wave method (FLAPW) in order to determine atomic magnetic moments and hyperfine fields for each Fe monolayer. As we can see from this figure there is a good agreement between theoretical and experimental values, despite the fact that the Fe counterpart for the former is the vacuum. In a recent calculation, Wu *et al.*[3] have determined magnetic moments and hyperfine fields for an Fe/Pt

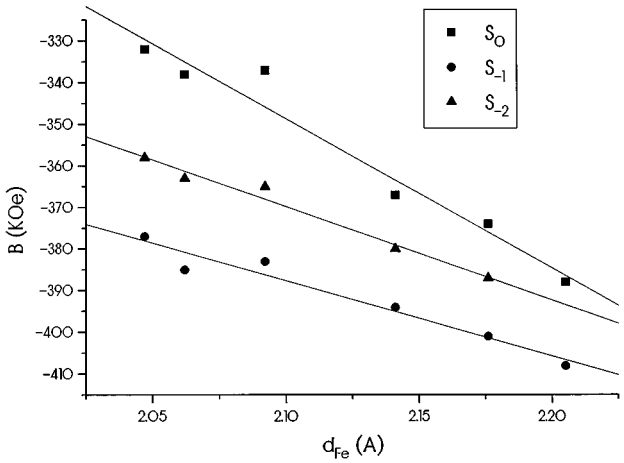

FIG. 13. Variation of the hyperfine field B assigned to individual Fe monolayers with the average lattice spacing d_{Fe} of the Fe layer for each of the x Å Fe/9 Å Pt samples.

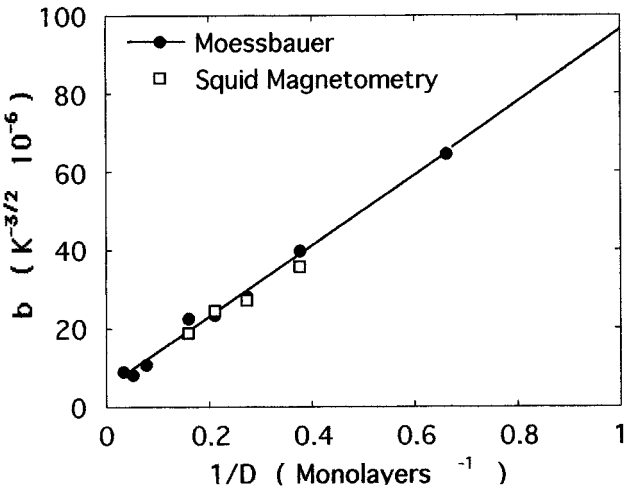

FIG. 14. Variation of the spin-wave stiffness constant b determined by Mössbauer (solid circles) and SQUID (open squares) data with the inverse Fe layer thickness for each of the x Å Fe/9 Å Pt samples. The solid line is a least square fit to the Mössbauer data.

multilayer with 5 Fe and 4 Pt monolayers. In this calculation they also employ the FLAPW technique but they let the system relax first. They obtained hyperfine field values of 275, 328, and 315 kOe for the S_0, S_{-1}, and S_{-2} monolayers, respectively, about 80 kOe smaller than the experimental values. The interplanar distances, as determined from the relaxation calculation, were 1.71 and 1.73 Å between the S_0 and S_{-1} and S_{-1} and S_{-2}, respectively. When they used more realistic interplanar spacings of 1.90 Å they calculated[20] hyperfine field values which were close to the experimental data, namely 356, 408, and 402 kOe, respectively. We have included these values also in Fig. 12. This sensitivity of the hyperfine field calculation to the interplanar spacings implies that the local spin density is substantially affected by these spacings. A careful inspection of Tables III and IV shows that the hyperfine fields for each individual monolayer decrease as the Fe layer thickness increases. According to the above observation this would imply a decrease of the corresponding interplanar distance. The structural refinement of the XRD data provides average Fe interplanar spacings within the Fe layer for each sample. As can be seen from Table I these spacings indeed decrease as the Fe layer thickness increases with constant Pt layer thickness. By plotting the hyperfine fields for each component assigned to the individual monolayers versus the average interplanar distance d_{Fe} for the samples with the same Pt thickness (Fig. 13) we get linear relations. These variations are in accordance with the decrease of the α-Fe hyperfine field in high pressure experiments.[21] Oscillatory d-spacing variations at interfaces have been predicted by Chen,[22] using a method of embedded atom method molecular dynamics and by Tsakalakos and Khachaturian[23] with analytical lattice statics.

So far we have seen that enhanced hyperfine fields and atomic magnetic moments with respect to bulk iron appear in the Fe/Pt multilayers investigated in this work. It appears from the above discussion that the interplanar distance and the Fe-Pt hybridization of the electronic wave functions are key factors for this enhancement. As was mentioned already, enhanced magnetization appears also in the so called ''high spin'' fcc Fe phase (which also exhibits lattice expansion), so our results could be also correlated with the existence of such a phase. The XAS and EXAFS data indicate the formation of such a phase for Fe layer thickness less than ~8 Å which transforms gradually to bcc as this thickness increases or the Pt layer thickness decreases. This gradual variation is apparent also in the hyperfine fields as shown in Tables III and IV. We must however stress the point that neither in the XAS and EXAFS data nor in the Mössbauer data a clear fcc phase appears. This result supports further our finding that the enhanced hyperfine fields are directly connected with the interplanar spacing.

As was mentioned in Sec. IV A, the spin-wave stiffness constant b decreases as the Fe layer thickness increases. We determined this constant also from the average hyperfine fields H_{av} for each sample by employing the relation

$$H_{\mathrm{av}}(T)=H_{\mathrm{av}}(4.2\ K)[1-bT^{3/2}]$$

and using the average values determined at RT and LHe. By plotting these values versus the inverse of the Fe layer thickness D^{-1} (Fig. 14) we get a linear relation with $b_0=5.0\times10^{-6}\ \mathrm{K}^{-3/2}$ which is very close to the bulk Fe value of $5.2\times10^{-6}\ \mathrm{K}^{-3/2}$. In the same graph we have included the b values calculated from the magnetization data which are in remarkable agreement with the values determined from the hyperfine field values. This agreement manifests the proportionality of the average hyperfine field and the magnetization for each sample.

VI. CONCLUSIONS

We have demonstrated in this work the possibility to determine the hyperfine field associated with each Fe monolayer in the Fe slab of the Fe/Pt system by employing standard Fe^{57} Mössbauer spectroscopy. The quality of the Fe/Pt multilayers studied in this work was a main factor for this achievement. The results show that the hyperfine field values follow an oscillatory variation as we move from the interface to the center of the Fe layer. This variation seems to depend on two factors: the hybridization of the $3d$ and $5d$ electron

wave functions and the variation of the interplanar spacing within the Fe layer. The importance and the role of each of these two factors remain to be further clarified.

ACKNOWLEDGMENTS

The authors wish to thank Constantin Chassapis for his assistance in preparing the structural refinement data. The authors are also thankful to Professor Wu and Professor Kioussis for the many valuable discussions of their band structure theoretical treatment of the Fe/Pt multilayers. T. T. wishes to acknowledge the support of DOE Grant No. DE-FG 05-90ER45430, A. J. the support of DOE at LLNL, and E. D. the European ERB SCI*CT 0050011 and HCM 930084 contracts. Finally A. S., E. D., and T. T. acknowledge the support of the Greek General Secretariat for R and D through the PENED programme.

[1] G. Kisters *et al.*, Hyperfine Interact. **92**, 285 (1994).
[2] A. J. Freeman and C. L. Fu, J. Appl. Phys. **61**, 3356 (1987).
[3] R. Wu, L. Chen, and N. Kioussis, J. Appl. Phys. **79**, 4783 (1996).
[4] T. Katayama *et al.*, J. Appl. Phys. **69**, 5658 (1991).
[5] M. Sakurai *et al.*, J. Magn. Magn. Mater. **147**, 16 (1995).
[6] B. M. Lairson *et al.*, Appl. Phys. Lett. **62**, 639 (1993).
[7] R. A. Brand *et al.*, J. Magn. Magn. Mater. **126**, 248 (1993).
[8] A. F. Jankowski, G. D. Waddill, and J. G. Tobin, J. Vac. Sci. Technol. **12**, 1215 (1994); in *Magnetic Ultrathin Films, Multilayers and Surfaces/Interfaces and Characterization*, edited by B. T. Jonker, S. A. Chambers, R. F. C. Farrow, C. Chappert, R. Clarke, W. J. M. de Jonge, T. Egami, P. Grünberg, K. M. Krishnan, E. E. Marinero, C. Rau, and T. Tsunashima, MRS Symposia Proceedings No. 313 (Materials Research Society, Pittsburgh, 1993), p. 227.
[9] E. Devlin *et al.*, J. Magn. Magn. Mater. **120**, 236 (1993).
[10] J. Korecki and U. Gradman, Phys. Rev. Lett. **55**, 2491 (1985).
[11] V. L. Moruzzi *et al.*, Phys. Rev. B **34**, 1786 (1984).
[12] R. D. Ellerbrock *et al.*, Phys. Rev. Lett. **74**, 3053 (1995).
[13] D. J. Keavney *et al.*, Phys. Rev. Lett. **74**, 4531 (1995).
[14] K. Chassapis and T. Tsakalakos, Comput. Phys. Commun. (to be published).
[15] M. Croft *et al.* (unpublished).
[16] M. B. Stearns, Phys. Rev. **167**, 439 (1966).
[17] J. Hesse, G. Nolle, and H. Korner, Solid State Commun. **46**, 721 (1983).
[18] K. Sumiyama *et al.*, J. Phys. F. **8**, 1281 (1978).
[19] Ch. Sauer (unpublished).
[20] N. Kioussis (private communication).
[21] R. D. Taylor and M. P. Pasternak, J. Appl. Phys. **69**, 6126 (1991).
[22] S. P. Chen, J. Mater. Sci. Eng. B **6**, 113 (1990).
[23] T. Tsakalakos and A. Khachaturyan, J. Mater. Sci. Eng. B **6**, 123 (1990).